Atmos. Chem. Phys. Discuss., doi:10.5194/acp-2017-256, 2017
Manuscript under review for journal Atmos. Chem. Phys.
Discussion started: 2 May 2017

Potential Influences of Neglecting Aerosol Effects on the NCEP GFS Precipitation Forecast

Mengjiao Jiang[1,2], Jinqin Feng[3], Ruiyu Sun[4], Zhanqing Li[1,2*], Bingcheng Wan[5], Maureen Cribb[2]

1, State Key Laboratory of Earth Surface Processes and Resource Ecology, College of Global Change and Earth System Science, Beijing Normal University, Beijing, China

2, Department of Atmospheric and Oceanic Science and ESSIC, University of Maryland, College Park, Maryland, USA

3, Longyan Meteorological Office of Fujian Province, Longyan, Fujian, China

4, IMSG, Environmental Modeling Center, National Centers for Environmental Prediction, National Oceanic and Atmospheric Administration, USA

5, State Key Laboratory of Atmospheric Boundary Layer Physics and Atmospheric Chemistry, Institute of Atmospheric Physics, Chinese Academy of Sciences, Beijing, China

Correspondence to:

Z. Li,

zli@atmos.umd.edu

Atmos. Chem. Phys. Discuss., doi:10.5194/acp-2017-256, 2017
Manuscript under review for journal Atmos. Chem. Phys.
Discussion started: 2 May 2017

Abstract

Aerosol-cloud interactions (ACI) have been widely recognized as a factor affecting precipitation. However, they have not been considered in the operational National Centers for Environmental Predictions Global Forecast System model. We evaluated the potential impact of neglecting ACI on the operational rainfall forecast using ground-based and satellite observations, and model reanalysis. The Climate Prediction Center unified gauge-based precipitation analysis and the Modern-Era Retrospective analysis for Research and Applications, Version 2 aerosol reanalysis were used to evaluate the forecast in three countries for the year 2015. The overestimation of light rain (47.84%) and underestimation of heavier rain (31.83%, 52.94%, and 65.74% for moderate rain, heavy rain, and very heavy rain, respectively) from the model are qualitatively consistent with the potential errors arising from not accounting for ACI, although other factors cannot be totally ruled out. The standard deviation of the forecast bias is significantly correlated with aerosol optical depth in Australia, the U.S., and China. To gain further insight, we chose the province of Fujian in China to pursue a more insightful investigation using a suite of variables from gauge-based observations of precipitation, visibility, water vapor, convective available potential energy (CAPE), and satellite datasets. Similar forecast biases were found: over-forecasted light rain and under-forecasted heavy rain. Long-term analyses reveal an increasing trend of heavy rain in summer, and a decreasing trend of light rain in other seasons, accompanied by a decreasing trend in visibility, no trend in water vapor,

and a slight increasing trend in summertime CAPE. More aerosols decreased cloud effective radii for cases where the liquid water path was greater than 100 g m^{-2}. All findings are consistent with the effects of ACI, i.e., where aerosols inhibit the development of shallow liquid clouds and invigorate warm-base mixed-phase clouds (especially in summertime), which in turn affects precipitation. While we cannot establish rigorous causal relations based on the analyses presented in this study, the significant rainfall forecast bias seen in operational weather forecast model simulations warrants consideration in future model improvements.

Atmos. Chem. Phys. Discuss., doi:10.5194/acp-2017-256, 2017
Manuscript under review for journal Atmos. Chem. Phys.
Discussion started: 2 May 2017

Atmospheric Chemistry and Physics Discussions

1. Introduction

Aerosols affect precipitation by acting as cloud condensation nuclei (CCN) and ice nuclei (IN), which can influence cloud microphysics (Twomey et al., 1984) and cloud lifetime (Albrecht, 1989). By absorbing and scattering radiation in the atmosphere, aerosols can alter the thermal and dynamic conditions of the atmosphere. The two types of effects are broadly referred to as aerosol-cloud interactions (ACI) and aerosol-radiation interactions (ARI) (Intergovernmental Panel on Climate Change, 2013). Both can influence precipitation (Rosenfeld et al., 2008) and many other meteorological variables to the extent that they may account for the considerable changes in climate experienced in Asia over the past half century (Li et al., 2016).

The impact of aerosols on precipitation via cloud microphysics occurs through warm-rain and cold-rain processes, as reviewed by Tao et al. (2012). In the warm-rain process, the competition for water vapor leads to a greater number of cloud drops with smaller sizes as the aerosol loading increases. This decreases the collision efficiency because of the low fall speed and low droplet-collecting efficiency. Rain formation is thus slowed down. In addition, a heavier aerosol loading narrows the cloud drop-size spectrum, lowering the coalescence and collision efficiencies. In the cold-rain process, the delay in precipitation formation from the warm-rain process enhances condensation and freezing, and ultimately, leads to the release of extra latent heat above the 0^{o}C isotherm (Andreae et al., 2004; Rosenfeld et al., 2008), favoring mixed-phase and cold rainfall processes. ARI also affect precipitation. First, solar radiation absorbed by aerosols may warm up a cloud droplet enough to evaporate it

Atmos. Chem. Phys. Discuss., doi:10.5194/acp-2017-256, 2017
Manuscript under review for journal Atmos. Chem. Phys.
Discussion started: 2 May 2017

(Ackerman et al., 2000). Second, heating of an aerosol layer due to absorption and cooling of the surface because of the reduction in radiation reaching the ground stabilizes the lower boundary-layer atmosphere and suppresses the formation and development of low clouds whose occurrence decreases with increasing aerosol loading (Li et al., 2011). The combination of ARI and ACI leads to a non-monotonic response of rainfall to aerosols: increasing first and then decreasing (Jiang et al., 2016) because the ACI and ARI are most significant for low and high aerosol loadings, respectively (Rosenfeld et al., 2008; Koren et al., 2008; Fan et al., 2016).

Most findings concerning the aerosol suppression of clouds and precipitation are associated with stratocumulus clouds, cumulus clouds, and shallow convection (Albrecht, 1989; Rosenfeld 2000; Jiang et al., 2006; Xue and Feingold, 2006; Khain et al., 2008), whereas those of enhanced rainfall are from deep convective clouds (Koren et al., 2005; Lin et al., 2006; Bell et al., 2008; Rosenfeld et al., 2008). Li et al. (2011) used 10 years of ground-based observations to examine the long-term impact of aerosols on precipitation and found rainfall enhancement in mixed-phase warm-base clouds and suppression in liquid clouds. Van den Heever et al. (2011) underlined the importance of cloud type in dealing with the impact of aerosols on precipitation.

Forecasting rainfall is most challenging and important in numerical weather prediction (NWP). In the current Global Forecast System (GFS) model, aerosols are only considered in the radiation scheme on a climatological scale. ARI are only considered offline and are not coupled with the dynamic system. ACI have not been accounted. To improve the forecast accuracy, a suite of new physical schemes are being implemented in the National Centers for Environmental Prediction (NCEP)'s Next-Generation Global Prediction System (NGGPS). The goal of modifying the current forecast model is to improve physical parameterizations in such a way that allows for efficient, accurate, and more complete representations of physical processes and their interactions including at least some of the aforementioned mechanisms.

As a first step, the goal of the present study is to evaluate current operational GFS forecast results (before any ACI are introduced) to see if any systematic precipitation biases bear resemblance to aerosol perturbations. A gross evaluation of the GFS model forecast results in three countries (China, the U.S, and Australia) were chosen, for they cover eastern and western hemispheres, northern and southern hemispheres, and represent highly different atmospheric and environmental conditions. Moreover, there are ARM observations in all three countries which will be used in follow-on studies to gain a deeper insight of causal relationships and the impact of different parameterization schemes. Descriptions of the operational GFS model, datasets, and the evaluation strategy and statistical method used are presented in section 2. Results of the evaluation and possible explanations are given in section 3. A summary of the research and discussion are given in Section 4.

2. Model, Datasets, and Methodology

2.1 Description of the NCEP GFS Model

2.1.1 Model Basics

The NCEP GFS model is a global spectral (spherical harmonic basis functions) model. The horizontal resolution is spectral triangular 1534 (T1534), or approximately 13 km at the equator for days 0–10, and spectral triangular 574 (T574), or approximately 34 km at the equator for days 10–16. The vertical domain is divided into 64 sigma-pressure hybrid (Sela, 2009) layers with enhanced resolution near the bottom and top (the top centered at about 0.27 hPa). The GFS model is based on the primitive equations, which include vorticity and divergence equations, the mass continuity equation, the hydrostatic equation, the thermodynamic equation, and the water vapor equation with parameterizations for atmospheric physics (Kanamitsu, 1989; Yang et al., 2006). A prognostic cloud water scheme (Sundqvist et al., 1989; Zhao and Carr, 1997; Moorthi et al., 2001) was added in May 2001.

2.1.2 Radiation

Shortwave and longwave radiation are parameterized using the Rapid Radiative Transfer Models (RRTMG) RRTMG_SW (v2.3) and RRTMG_LW (v2.3), respectively, developed at AER Inc. (http://www.emc.ncep.noaa.gov/GFS/doc.php). A Monte Carlo independent column approximation method is used in the RRTMG to deal with multi-layered clouds and a maximum-random cloud overlapping method is assumed for radiative calculations (http://www.emc.ncep.noaa.gov/GFS/doc.php) whose soundness has been assessed (Yoo et al., 2013). The cloud cover calculation for radiation, which follows Xu and Randall (1996), was also modified because it

Atmos. Chem. Phys. Discuss., doi:10.5194/acp-2017-256, 2017
Manuscript under review for journal Atmos. Chem. Phys.
Discussion started: 2 May 2017

Atmospheric Chemistry and Physics Discussions

produced too much low cloud globally (Yoo et al., 2012, 2013). A monthly climatology of aerosols composed of five primary species similar to that in the Goddard Chemistry Aerosol Radiation and Transport model (GOCART) was used. One or two major components were chosen for both longwave and shortwave radiative transfer calculations.

2.1.3 Planetary Boundary Layer

In the planetary boundary layer (PBL), a hybrid eddy-diffusivity mass flux PBL parameterization (Han et al., 2016) was incorporated to replace the previous PBL scheme, which was originally proposed by Troen and Mahrt (1986) (http://www.emc.ncep.noaa.gov/GFS/doc.php) and implemented by Hong and Pan (1996). The PBL scheme was modified to improve daytime PBL growth (http://www.emc.ncep.noaa.gov/GFS/doc.php).

2.1.4 Convection

A modified version (Han and Pan, 2011) of the Simplified Arakawa-Schubert scheme (Arakawa and Schubert, 1974; Grell, 1993; Pan and Wu, 1995) is used for deep convection in the GFS model. Water substance (liquid) detrained from the cloud top is a source term of the prognostic cloud mixing ratio. The new shallow convection scheme (Han and Pan, 2011) uses a bulk mass-flux parameterization, which is similar to the deep convection scheme, but with a cloud-top limit of 700 hPa and different specifications on entrainment, detrainment, and mass flux at the cloud base. The detrained liquid water in updrafts is allowed to become convective rain (although the precipitation from shallow convection is small) and grid-scale cloud condensate (Han and Pan, 2011).

2.1.5 Precipitation

The cloud condensate has two sources: large-scale condensate (based on Zhao and Carr (1997)), and convective condensation, which is from convective detrainment. Convective precipitation is calculated from convection. Grid-scale precipitation is the sink of cloud condensate and is diagnostically calculated from cloud condensate. It is parameterized following Zhao and Carr (1997) for ice (snow), evaporation of rain and snow, and the melting of snow, and following Sundvist et al. (1989) for liquid water (rain) (GCWM Branch, EMC, 2003).

2.2 Descriptions of Datasets Used

Datasets used include Modern-Era Retrospective analysis for Research and Applications, Version 2 (MERRA-2) aerosol optical depth (AOD) data, Climate Prediction Center (CPC) unified gauge-based precipitation data, and the NCEP GFS precipitation forecast data for the year 2015 in three countries: China, the U.S., and Australia. Other datasets used include long-term NCEP Global Ensemble Forecast System (GEFS) precipitation forecast data, ground-based observations of precipitation and visibility, water vapor and convective available potential energy (CAPE) sounding datasets, and satellite-retrieved aerosol and cloud properties for a small

Atmos. Chem. Phys. Discuss., doi:10.5194/acp-2017-256, 2017
Manuscript under review for journal Atmos. Chem. Phys.
Discussion started: 2 May 2017

region of Fujian Province in China chosen for more detailed study.

2.2.1 NASA MERRA-2 Aerosol Reanalysis

The MERRA-2 is the second generation of the MERRA reanalysis (Rienecker et al., 2011). The biggest differences between the first and second versions of MERRA is that the new generation of MERRA uses an updated model (Molod et al., 2012, 2015) and a global statistical interpolation analysis scheme (Wu et al., 2002). This enables the system to include new data types. MERRA-2 takes account of analyzed and modeled aerosol fields with radiative effects that respond to the meteorological field (Randles et al., 2016). The MERRA-2 aerosol reanalysis is an upgrade of the off-line aerosol reanalysis called MERRAero (da Silva et al., 2011; Jiang et al., 2016). The aerosol module in MERRAero is based on the GOCART model (Chin et al., 2002). The bias-corrected AOD is retrieved from Moderate Resolution Imaging Spectroradiometer (MODIS) observations. Cloud-screened AERONET AOD data are used in the neural network to integrate MODIS radiances into bias-corrected AODs. The MERRA-2 aerosol reanalysis includes additional measurements from the NASA Earth Observing System, NOAA Polar Operational Environmental Satellites, and ground-based observations (Randles et al., 2016). Bias-corrected AODs from satellite and Aerosol Robotic Network (AERONET) AODs have been added in the assimilation (Randles et al., 2016).The AOD observing system sensors extend from the MODIS Neural Net Retrieval (NNR) in MERRAero to a combination of the Advanced Very-High-Resolution Radiometer NNR, AERONET, the Multi-angle

Imaging SpectroRadiometer, the MODIS/Terra NNR, and the MODIS/Aqua NNR in the MERRA-2 aerosol reanalysis. More details about the MERRA-2 aerosol reanalysis can be found in Randles et al. (2016). Hourly total aerosol extinction AOD data at 550 nm for the year 2015 are used in this study.

2.2.2 CPC Unified Gauge-based Analysis of Global Daily Precipitation

A unified suite of precipitation analysis products were assembled at NOAA's CPC that ingest a gauge-based analysis of global daily precipitation over land (https://climatedataguide.ucar.edu/climate-data/cpc-unified-gauge-based-analysis-global-daily-precipitation). Over 30,000 station reports were first collected from multiple sources. Quality control was performed through comparisons with other sources of data, e.g., from radar, satellite, numerical models, independent nearby stations, and historical precipitation records. Post-quality control corrected reports are interpolated to create the analyzed fields. Orographic effects are considered in this step (Xie et al., 2007). Finally, the daily analysis is constructed and released at a 0.5^{o} x 0.5^{o} resolution (https://climatedataguide.ucar.edu/climate-data/cpc-unified-gauge-based-analysis-global-daily-precipitation). Daily precipitation data for the year 2015 are used in this study.

2.2.3 NCEP GFS/GEFS Forecast Datasets

The NWP model forecast data employed are three-hourly rainfall forecasts from the NCEP GFS model initialized at 0000 coordinated universal time (UTC) and accumulated for 24 hours in the three countries chosen for study. The mean cloud mixing ratio at 850 hPa corresponding to the precipitation record in the U.S. at a 0.5°x0.5° latitude-longitude resolution for the year 2015 is also used in the analysis. For the part of the study focused on Fujian Province, China, the NWP model reforecast precipitation amount accumulated over the period of 12 hours to 36 hours out from the 0000 UTC run at six-hourly intervals at a 1°x1° latitude-longitude resolution for the years 1985 to 2010 are used to calculate the modeled daily precipitation amount in each grid box. They are interpolated to match with long-term ground-based precipitation observations recorded at each of the 67 stations in the study region of Fujian, China (Fig. 1).

2.2.4 Long-term Ground-based Observations in Fujian Province, China

Ground meteorological data acquired in Fujian Province from 1980 to 2009 are used in this study. Figure 1 shows the locations of the 67 meteorological stations measuring precipitation. Sixteen of these stations also collect visibility data four times a day. Daily mean data are employed here. Serving as a proxy for aerosol loading, visibility was corrected for relative humidity (RH) (Charlson, 1969; Appel et al., 1985) using the formula adopted by Rosenfeld et al. (2007) when RH falls between 40% and 99%:

$$\frac{V_{ori}}{V_{cor}} = 0.26 + 0.4285\, lg(100 - RH), \quad (1)$$

where RH is in percent, and V_{ori} and V_{cor} are the originally uncorrected and corrected visibilities, respectively. Only non-rainy data were used.

Atmos. Chem. Phys. Discuss., doi:10.5194/acp-2017-256, 2017
Manuscript under review for journal Atmos. Chem. Phys.
Discussion started: 2 May 2017

Atmospheric Chemistry and Physics Discussions

To analyze water vapor and atmospheric stability effects on precipitation, data from three atmospheric sounding stations (Xiamen, 24.48°N, 118.08°E; Shaowu, 27.33°N, 117.46°E; Fuzhou, 26.08°N, 119.28°E) are used to calculate trends in precipitable water vapor and CAPE. Daily precipitable water and CAPE values are the mean of the two measurements made per day.

2.2.5 Satellite Datasets of Aerosol and Cloud Properties in Fujian Province, China

CloudSat data from 2006–2010 amassed over Fujian Province (22.5°N-28.5°N, 114.5°E-120.5°E) are used to extract cloud-top and cloud-base height information. CloudSat retrievals of cloud-top and base heights are converted to temperatures using temperature profiles from the European Center for Medium-range Weather Forecasting Auxiliary product. The converted cloud-top and cloud-base temperatures are used for cloud type classification. The classification of different cloud types is summarized in Table 1 and introduced in sub-section 2.3.1. Only single-layer clouds detected by the CloudSat are chosen here.

Aqua/MODIS retrievals of cloud droplet size and liquid water path (LWP) for liquid clouds (clouds with cloud-top temperatures (CTT) greater than 273 K) from 2003–2012 collected over Fujian Province are used. The MODIS Level 3 AOD at 550 nm product is also used. Grid boxes with AOD > 0.6 are excluded in this study to reduce the possibility of cloud contamination in AOD retrievals.

2.3 Methodology

2.3.1 Rainfall Level Classification and Cloud Type Classification

Based on the definitions of the China Meteorological Administration, precipitation data are classified into four groups according to the daily rain amount: light rain (0.1–9.9 mm d^{-1}), moderate rain (10–24.9 mm d^{-1}), heavy rain (25–49.9 mm d^{-1}), and very heavy rain ($\geqslant$ 50 mm d^{-1}).

Table 1 summarizes the cloud types considered in the long-term analysis for Fujian Province. Deep mixed-phase clouds are defined as clouds with cloud-base temperatures (CBT) > 15°C and cloud-top temperatures (CTT) < -4°C, shallow mixed-phase clouds are defined as clouds with CBT ranging from 0°C to 15°C and CTT < -4°C, and pure liquid clouds are defined as clouds with CBT > 0°C and CTT > 0°C (Li et al., 2011; Niu and Li, 2012).

2.3.2 Evaluation Methods

Quantitative precipitation forecast scores developed by NCEP are used in the evaluation. Table 2 is a contingency table based on documents from the World Climate Research Programme (http://www.cawcr.gov.au/projects/verification/#Methods_for_dichotomous_forecasts). The most commonly-used statistical scores are the equitable threat score (ETS), which is also called the Gilbert skill score, and the bias score (BIAS). The ETS is given by

$$ETS = \frac{H-H_{random}}{H+m+f-H_{random}}, \qquad (2)$$

where H represents hits, f represents false alarms, and m represents misses. H_{random} is given by

$$H_{random} = \frac{(H+m)*(H+f)}{TOTAL}. \quad (3)$$

Its values range from -1/3 to 1 and a perfect score is 1. The BIAS is expressed as

$$BIAS = \frac{H+f}{H+m}. \quad (4)$$

Its values range from 0 to infinity. A perfect score is 1. A BIAS < 1 indicates under-forecasting and a BIAS > 1 indicates over-forecasting.

To obtain the forecast skill under a particular pollution condition, the ETS and the BIAS for each AOD range are calculated as

$$< ETS >_{i,j,m} = (ETS)_{i,j,m}, \quad (5)$$

$$< BIAS >_{i,j,m} = (BIAS)_{i,j,m}, \quad (6)$$

for the index of precipitation threshold i, cloud mixing ratio j, and AOD bin m.

2.3.3 Statistical Method

The standard deviation of the precipitation bias between the GFS model and CPC gauge data is calculated as

$$S = \sqrt{\frac{\Sigma(x-r)^2}{n-1}}\ , \quad (7)$$

where x is the forecast bias on a single day, n is equal to 364 days, and r is the mean forecast bias. The Pearson's method is used to calculate the linear correlation coefficient of the relationship between the standard deviation of the forecast difference and AOD. A t-test is applied with the p value set to 0.05.

The relative difference between the forecast precipitation and observations is

Atmos. Chem. Phys. Discuss., doi:10.5194/acp-2017-256, 2017
Manuscript under review for journal Atmos. Chem. Phys.
Discussion started: 2 May 2017

Atmospheric Chemistry and Physics
Discussions

calculated as

$$\Delta P = \frac{P_{GFS/GEFS} - P_{OBV}}{P_{OBV}} \times 100\%, \qquad (8)$$

where $P_{GFS/GEFS}$ refers to the forecast precipitation and P_{OBV} refers to the precipitation from gauge-based observations.

For the long-term analysis, trends in a particular parameter are defined as the relative change in the parameter (in %) over each successive decade (Lin and Zhao, 2009). The Mann-Kendall method is used to test the significance of the trend.

3. Results

3.1 Evaluation of GFS Precipitation using the CPC Gauge-based Analysis

3.1.1 Annual Mean Patterns

The CPC gauge-based precipitation analysis from 2015 is used to evaluate the GFS precipitation forecast. Figure 2 shows the annual mean precipitation difference between the GFS model and the CPC analysis for three countries, i.e., China, the U.S., and Australia, for the year 2015. Values above (below) zero represent the overestimation (underestimation) of precipitation. In China (Figure 2a), the GFS model overestimates the mean daily rainfall mostly in southwest China, especially in Sichuan, Yunnan, and Guizhou Provinces (by ~3 mm d^{-1}), and in northwest China, where rain events are scarcer. Rainfall is underestimated over the Yangtze River Delta region and the eastern coast of China. In the U.S. (Figure 2b), the GFS model overestimates precipitation by about 1–2 mm d^{-1} in most regions and underestimates precipitation along the coastline of the Gulf of Mexico (by ~1 mm d^{-1}). In Australia

(Figure 2c), the forecast performance is good. In northern Australia, the underestimation of precipitation is around 2 mm d^{-1}. Z-scores were calculated to test the significance of the annual mean difference in the daily rainfall amount between the GFS model forecast and the CPC analysis. Z values range from -0.4803 to 0.8534 over the grids in the three countries. Because the Z-score values are less than 2, this indicates that the mean difference is not significant at the two-sigma level. Therefore, the forecast performance of the GFS model with regard to the annual mean daily rainfall in the three countries is sound with reference to the gauge-based CPC rainfall analysis.

3.1.2 Different Rainfall Intensities

Figure 3 shows the annual mean relative difference between forecast precipitation and observations for light rain (0–10 mm d^{-1}) and heavier rain (> 10 mm d^{-1}). The GFS model overestimates light rain in most places (Figure 3a) and underestimates heavier rain (Figure 3b). This suggests that both the overestimation of light rain and underestimation of moderate rain, heavy rain and very heavy rain contribute to the forecast bias. Figure 4 shows the mean relative difference between forecast and observed daily precipitation amounts for different rain intensities in the three countries for whole year (Fig. 4a) and for summer only (Fig. 4b). GFS forecasts overestimate light rain by 47.84% and underestimate moderate rain, heavy rain, and very heavy rain by 31.83%, 52.94%, and 65.74%, respectively (Fig. 4a). The underestimation of precipitation in summer is larger for moderate rain (32.93%), heavy rain (55.19%), and very heavy rain (66.93%, Fig. 4b). Of course, these model biases are caused by many factors, and it's beyond the scope of this paper to explore all possible causes. Our focus is on any potential contribution by neglecting aerosol effects to the biases. The relationship between model performance and AOD is thus further investigated.

3.1.3 Relationship between Model Performance and AOD

In principle, the underestimation and overestimation at different rainfall levels (Figs. 3 and 4) may be linked to AOD conditions, as elaborated in the introduction of previous studies (c.f. the review of Tao et al., 2012). The standard deviation of the forecast bias at each grid point in the three countries is calculated to further examine the links between the model bias and AOD， as aerosols tend to polarize precipitation by suppressing light rain and enhancing heavy rain and thus increase the standard deviation. The calculation of the standard deviation of the forecast difference is based on Eqn. (7). Figure 5 shows the relationship between the standard deviation and AOD in the three countries. Each point represents a grid box. The standard deviation and AOD has a significant positive correlation in the three countries with correlation coefficients of 0.5602, 0.6522, and 0.5182 for Australia, the U.S., and China, respectively. This suggests that the degree of disparity of the forecast error is larger for regions with high aerosol loading. The slopes of the best-fit lines are 75.23 for relatively clean Australia (maximum AOD < 0.18), 48.4 for the polluted U.S. (maximum AOD < 0.20), and 8.554 for heavily polluted China (maximum AOD >

0.60).

The ETS and BIAS are used to examine the model performance in different AOD bins for certain cloud mixing ratio conditions in the U.S. (Fig. 6). In Figs. 6a and 6b, when the threshold is set to 5 mm d^{-1}, the ETS increases as the cloud mixing ratio increases. This happens because large-scale precipitation is diagnostically calculated from cloud mixing ratios. The ETS decreases as AOD increases except under low cloud mixing ratio conditions. However, the BIAS shows little change as AOD or the cloud mixing ratio changes. In Figs. 6c and 6d, when the threshold is set to 20 mm d^{-1}, the ETS also increases as cloud mixing ratio increases. The ETS decreases as AOD increases under all cloud mixing ratio conditions. This suggests that the AOD influences the model rainfall forecast especially for stronger levels of precipitation. The decreases in BIAS score with AOD (Fig. 6d) also shows that the underestimation for heavy rainfall increases as AOD increases for low and middle cloud mixing ratio conditions.

3.2 Potential Contribution of Aerosols to the Model Bias

3.2.1 Long-term Forecast Bias and Trends in Observed Precipitation in Fujian Province, China

The model performance differs under different conditions, e.g., initial and dynamic settings, and weather regimes. A long-term statistical evaluation of rainfall forecasts for Fujian Province is made to mitigate these fluctuations in the model forecast accuracy. Model data from 1985 to 2010 are used to calculate the relative difference based on Eqn. (8). Figure 7 shows the mean relative difference between forecast and observed precipitation for different rain rates from the 67 stations in Fujian Province for all seasons and for summer only. Figure 7a shows that there is 114.36% more precipitation forecast by the NCEP/GEFS model than observed for the light rain cases. For moderate rain, heavy rain, and very heavy rain cases, 29.20%, 41.74%, and 59.30% less precipitation than observed, respectively, was forecasted. The underestimation of moderate rain (46.88%), heavy rain (59.58%), and very heavy rain (70.16%) is even larger in summer (Fig. 7b).

Seasonally-averaged trends (percent change per decade) in daily rain amount and frequency over Fujian Province from 1980 to 2009 are calculated. Only the results for rain amount are shown in Fig. 8 because the frequency results bear a close resemblance. Cross-hatched bars represent data at a confidence level greater than 95%. In spring, daily rain amounts decreased over time, ranging from -4.9% to -15.3% per decade for different rain rates. In summer, heavy and very heavy daily rain amounts increased significantly. For very heavy rain, the amount and frequencies increased at a rate of 21.8% and 24.5% (not shown), respectively. In autumn, light rain and moderate rain amounts decreased. In winter, the light rain amount decreased over time. Decreases in light rain amounts are -8.4% per decade. Overall, the increasing trends in summertime for heavy and very heavy rain are most significant. The decreasing trends in light rain in other seasons are also significant.

3.2.2 Examination of Potential Contributors

Atmos. Chem. Phys. Discuss., doi:10.5194/acp-2017-256, 2017
Manuscript under review for journal Atmos. Chem. Phys.
Discussion started: 2 May 2017

Reasons for the difference between modeled and observed precipitation are examined in terms of aerosol effects, water vapor, and CAPE. The time series of visibility over the period of 1980–2009 are shown in Fig. 9. Visibility has declined steadily in all seasons but summer during which there was a short-lived increasing trend from 1992–1997. The linear declining trends are statistically significant at the 95% confidence level. The greatest reduction is seen during the summer, especially after 1997. Tables 3 and 4 summarize the correlation between visibility and precipitation amount and frequency, respectively. A positive (negative) correlation between visibility and precipitation means a negative (positive) correlation between aerosol concentration and precipitation. Values with an asterisk represent data at a confidence level greater than 95%. For light rain, the correlations between daily rain amount and visibility (Table 3) and between rain frequency and visibility (Table 4) are positive for all seasons. For heavy rain to very heavy rain, the correlations between visibility and daily rain amount (Table 3), as well as frequency (Table 4), are negative in summer.

Water vapor amount and atmospheric stability are important factors related to precipitation. To analyze the potential contributions of these factors to the forecast bias, their effects on precipitation are examined. Data from three atmospheric sounding stations (Xiamen, 24.48°N, 118.08°E; Shaowu, 27.33°N, 117.46°E; Fuzhou, 26.08°N, 119.28°E) collected from 1980–2009 are used to calculate trends in precipitable water vapor and CAPE. Figure 10 shows time series of annual mean water vapor amount for different seasons. A slight increasing trend is seen in winter,

Atmos. Chem. Phys. Discuss., doi:10.5194/acp-2017-256, 2017
Manuscript under review for journal Atmos. Chem. Phys.
Discussion started: 2 May 2017

while no discernible trend is seen in other seasons. This suggests that the water vapor amount characterizing the study region cannot explain seasonal variations in precipitation. Time series of mean CAPE for the different seasons are shown in Fig. 11. There is an increasing trend in summertime CAPE during the period of 1980–2009, but the trends are not as strong in other seasons. The observed increase in rain amount in summer is in part likely due to an increase in convective precipitation events that arises from the increasing trend in CAPE.

3.2.3 Impact of Aerosols on Clouds and Precipitation

Aerosols can influence precipitation through warm- and cold-rain processes (Tao et al., 2012). Cloud droplet size, LWP for clouds with CTT greater than 273 K, and AOD at 550 nm retrieved from the Aqua/MODIS platform over Fujian Province during the period of 2003–2012 are used to examine the impact of aerosol on cloud effective radius (CER). Figure 12 shows CER as a function of AOD for liquid clouds with different LWPs. When the AOD is small (< 0.2), the CER increases with increasing LWP. For LWP > 100 g m^{-2}, the CER decreases with increasing AOD, which suggests that more aerosols decrease CERs. This result is in line with the two aerosol indirect effects (Twomey et al., 1984; Albrecht, 1989). A greater number of smaller droplets may reduce precipitation efficiency and suppress or enhance precipitation, as reviewed by Tao et al. (2012).

Several observational and model studies suggest that smaller cloud particles are more likely to ascend to above the freezing level, releasing latent heat and invigorating deep convection (Rosenfeld et al., 2008; Li et al., 2011) while suppressing shallow convection. Cloud top temperature (CTT) and cloud base temperature (CBT), converted from CloudSat measurements of cloud top and base heights, in Fujian Province from 2006 to 2010 are used to study the impact of aerosols on the cloud development of different clouds. Figure 13 shows CTT as a function of AOD for liquid and warm- and cold-base mixed-phase clouds. Definitions of the different cloud types are summarized in Table 1, which is taken from Li et al. (2011). Left-hand ordinates are for liquid clouds, while right-hand ordinates are for warm-base and cold-base mixed-phase clouds. For all seasons (Fig. 13a), CTTs of warm-base mixed-phase clouds are lower than those of cold-base mixed-phase clouds. Warm-base mixed-phase CTTs decrease with increasing AOD, which indicates that cloud-top heights have increased. For cold-base mixed-phase clouds, variations in CTT with AOD are not obvious. For liquid clouds, CTTs increase slightly with AOD, which means that the development of liquid clouds is suppressed when AOD increases. In summer, CTTs decrease more significantly with increasing AOD for warm-base mixed-phase clouds and increase more significantly with increasing AOD for liquid clouds (Fig. 13b). This suggests that aerosols inhibit the development of shallow liquid clouds and invigorate warm-base mixed-phase clouds, with little influence on cold-base mixed-phase clouds. These effects of aerosols on summertime cloud development are more obvious, likely because convective clouds occur more frequently during the summertime in Fujian Province.

These results agree with those from a ground-based study using Atmospheric

Radiation Measurement Southern Great Plains data (Li et al., 2011) and from a tropical region study using CloudSat/Cloud-Aerosol Lidar and Infrared Pathfinder Satellite Observation data (Niu and Li, 2012; Peng et al. 2016). The impact of aerosols on different types of clouds may lead to light rain suppression and heavier rain enhancement. If the model neglects aerosol effects, the forecast may result in overestimation for light rain and underestimation for heavy to very heavy rain. For example, Fig. 14 shows time series of regionally-averaged daily modeled and observed precipitation in 2001. Modeled and observed precipitation amounts over the region agree well in spring and winter while modeled precipitation amounts are greater than observations for light rain in autumn. Note that modeled precipitation amounts are significantly less than observed precipitation amounts over the region in summer when deep convective clouds and heavy to very heavy rain most likely occur. Although there are many reasons for the difference between modeled and observed precipitation, these results suggest that the neglect of aerosol effects may contribute to the model rainfall forecast bias to some extent.

Summary and Discussion

Aerosol-cloud interactions (ACI) have been recognized as playing a vital role in precipitation, but have not been considered in the National Centers for Environmental Prediction (NCEP) Global Forecast System model yet. For more efficient and accurate forecasts, new physical schemes are being incorporated into the NCEP's Next-Generation Global Prediction System. As a benchmark evaluation of model

Atmos. Chem. Phys. Discuss., doi:10.5194/acp-2017-256, 2017
Manuscript under review for journal Atmos. Chem. Phys.
Discussion started: 2 May 2017

results that exclude aerosol effects, the operational precipitation forecast (before any ACI are included) is evaluated using multiple datasets with the goal of determining if there is any link between the model forecast bias and aerosol loading. Multiple datasets are employed, including ground-based precipitation and visibility datasets, Aqua/Moderate Resolution Imaging Spectroradiometer products, CloudSat retrievals of cloud-base and cloud-top heights, Modern-Era Retrospective analysis for Research and Applications, Version 2 model simulations of aerosol optical depth (AOD), and GFS forecast datasets.

Operational daily precipitation forecasts for the year 2015 in three countries, i.e., Australia, the U.S., and China, were evaluated. The model overestimates light rain, and underestimates moderate rain, heavy rain, and very heavy rain. The underestimation of precipitation in summer is even larger. This is consistent qualitatively with expected results because the model does not account for aerosol effects on precipitation, i.e., the inhibition of light rain and enhancement of heavy rain by aerosols. The standard deviations of forecast differences are generally positively correlated with increasing aerosol loadings in the three countries. Equitable threat scores also decrease with increasing AOD, especially for heavier rain forecasts.

An analysis of long-term measurements from Fujian Province, China was done. Light rain overestimation, and moderate, heavy, and very heavy rain underestimations from the Global Ensemble Forecast System were also seen. The underestimation for stronger rainfall is larger in the summertime. Increasing trends for heavy and very heavy rain in summer, and decreasing trends for light rainfall in other seasons are significant from 1980 to 2009. Long-term analyses show that neither water vapor nor convective available potential energy can explain these trends. Satellite datasets amassed in Fujian Province from 2006 to 2010 were used to shed more light on the impact of aerosols on cloud and precipitation. As implied by the Twomey effect, cloud effective radius decreases with increasing AOD, which likely suppress light rain and enhance heavy rain. Both of them can contribute to some extent to the model forecast bias. The underestimation of heavy rain in summer most likely occurs because deep convective clouds occur more frequently during the summertime.

How neglecting ACI in the operational forecast model impacts model biases remains an open question. This study is arguably the first attempt at evaluating numerical weather prediction forecast errors in terms of the potential effects of aerosols. A more rigorous and systematic evaluation would require further insights into the model with rich instantaneous measurements to allow for case-based investigations that are under way.

Data Availability

Forecast data are from the NOAA NOMADS (https://nomads.ncdc.noaa.gov/) for GFS data (https://nomads.ncdc.noaa.gov/data/gfs4/) and the NOAA NCDC (https://www.ncdc.noaa.gov/data-access/model-data/model-datasets/global-ensemble-forecast-system-gefs) for GEFS reforecast data. NASA MERRA-2 aerosol data are accessible from the NASA Global Modeling and Assimilation Office (https://gmao.gsfc.nasa.gov/reanalysis/MERRA-2/data_access/). The CPC Unified

Gauge-Based Analysis of Global Daily Precipitation dataset is available at (https://climatedataguide.ucar.edu/climate-data/cpc-unified-gauge-based-analysis-global-daily-precipitation). ECMWF reanalysis data are accessible via http://apps.ecmwf.int/datasets/data/interim-full-daily/. MODIS data and CloudSat data are available at https://modis.gsfc.nasa.gov/data/ and http://www.cloudsat.cira.colostate.edu/, respectively. Ground-based observations of precipitation amount, visibility, precipitable water, and CAPE from Fujian Province can be requested from the Chinese Meteorological Administration's National Meteorological Information Center (http://cdc.cmic.cn and http://data.cma.cn/).

Acknowledgements

This study was supported by the Ministry of Science and Technology of China (2013CB955804), State Key Laboratory of Earth Surface Processes and Resource Ecology (2015-TDZD-090), and NOAA (NA15NWS4680011). We would like to thank the NASA Global Modeling and Assimilation Office (https://gmao.gsfc.nasa.gov/reanalysis/MERRA-2/data_access/) and the Goddard Space Flight Center Distributed Active Archive Center for their help in accessing MERRA-2 inst3_2d_gas_Nx: 2d, 3-Hourly, Instantaneous, Single-Level, Assimilation, Aerosol Optical Depth Analysis Version 5.12.4 data. We would also like to thank the staff at the National Center for Atmospheric Research responsible for creating the "The Climate Data Guide: CPC Unified Gauge-Based Analysis of Global Daily Precipitation" (https://climatedataguide.ucar.edu/climate-data/cpc-unified-gauge-based-analysis-glob al-daily-precipitation). Thanks also go to the NOAA NOMADS (https://nomads.ncdc.noaa.gov/) for GFS data (https://nomads.ncdc.noaa.gov/data/gfs4/), the NOAA NCDC (https://www.ncdc.noaa.gov/data-access/model-data/model-datasets/global-ensemble-forecast-system-gefs) for GEFS reforecast data, and the NWS CPC for data downloading software (http://www.cpc.ncep.noaa.gov/products/wesley/get_gfs.html). We acknowledge the Chinese Meteorological Administration's National Meteorological Information Center (http://cdc.cmic.cn and http://data.cma.cn/), the European Centre for Medium-Range Weather Forecasts (ECMWF) (http://www.ecmwf.int/), the NASA Goddard Space Flight Center (https://modis.gsfc.nasa.gov/data/), and the CloudSat Data Processing Center (http://www.cloudsat.cira.colostate.edu/) for providing the various datasets used in the study.

We would also like to thank Drs. Yu-Tai Hou, Shrinivas Moorthi, and Jun Wang from NOAA, Sarah Lu from State University of New York, Albany, Dr. Seoung-Soo Lee and Lei Zhang from the University of Maryland, and Dr. Duoying Ji from Beijing Normal University for their discussions regarding this study. We especially appreciate the help given by Drs. Yu-tai Hou, Jongil Han, and Yuejian Zhu in understanding the GFS/GEFS models and data products, and the guidance provided by Dr. Hye-Lim Yoo. We also greatly appreciate the valuable comments from the anonymous reviewers.

References

Ackerman, A. S., Toon, O. B. , Stevens, D. E., Heymsfield, A. J., Ramanathan, V., and Welton, E. J.: Reduction of tropical cloudiness by soot, Science, 288(5468), 1042–1047,

Atmos. Chem. Phys. Discuss., doi:10.5194/acp-2017-256, 2017
Manuscript under review for journal Atmos. Chem. Phys.
Discussion started: 2 May 2017

Atmospheric Chemistry and Physics
Discussions

doi:10.1126/science.288.5468.1042, 2000.

Albrecht, B. A.: Aerosols, cloud microphysics, and fractional cloudiness, Science, 245(4923), 1227–1230, doi:10.1126/science.245.4923.1227, 1989.

Andreae, M. O., Rosenfeld, D., Artaxo, P., Costa, A. A., Frank, G. P., Longo, K. M., and Silva-Dias, M. A. F.: Smoking rain clouds over the Amazon, Science, 303(5662), 1337–1342, doi:10.1126/science.1092779, 2004.

Appel, B. R., Tokiwa, Y., Hsu, J., Kothny, E. L., and Hahn, E.: Visibility as related to atmospheric aerosol constituents, Atmos. Environ., 19, 1525–1534, doi: 10.1016/j.bbr.2011.03.031, 1985.

Arakawa, A., and Schubert, W. H.: Interaction of a cumulus cloud ensemble with the large-scale environment. Part I. J. Atmos. Sci., 31, 674–701, doi:10.1175/1520-0469(1974)031<0674:IOACCE>2.0.CO;2, 1974.

Bell, T., Rosenfeld, D., Kim, K., Yoo, J., Lee, M., and Hahnenberger, M.: Midweek increase in U.S. summer rain and storm heights suggests air pollution invigorates rainstorms, J. Geophys. Res. Atmos., 113, D02209, doi:10.1029/2007JD008623, 2008.

Charlson, R. J.: Atmospheric visibility related to aerosol mass concentration: Review, Environ. Sci. Technol., 3, 913–918, doi:10.1021/es60033a002, 1969.

Chin, M., Ginoux, P., Kinne, S., Torres, O., Holben, B., Duncan, B. N., Martin, R. V., Logan, J., Higurashi, A., and Nakajima, T.: Tropospheric aerosol optical thickness from the GOCART model and comparisons with satellite and Sun photometer measurements, J. Atmos. Phys., 59, 461–483, doi:10.1175/1520-0469(2002)059<0461:TAOTFT>2.0.CO;2, 2002.

da Silva, A., Colarco, P. R., Darmenoy, A. S., Buchard-Marchant, V., Randles, C. A., and Gupta, P.: An overview of the GEOS-5 Aerosol Reanalysis, American Geophysical Union, Fall Meeting 2011, abstract #A52D-09, San Francisco, CA, USA, 2011.

Fan, J. W., Wang, Y., Rosenfeld, D., and Liu, X.: Review of aerosol–cloud interactions: mechanisms, significance, and challenges, J. Atmos. Sci., 73(11), 4221–4252, doi:10.1175/JAS-D-16-0037.1, 2016.

GCWM Branch, EMC: The GFS atmospheric model. NCEP Office Note 442, 14 pp., available at: http://wwwt.emc.ncep.noaa.gov/officenotes, 2003.

Grell, G. A.: Prognostic evaluation of assumptions used by cumulus parameterizations, Mon. Wea.

Atmos. Chem. Phys. Discuss., doi:10.5194/acp-2017-256, 2017
Manuscript under review for journal Atmos. Chem. Phys.
Discussion started: 2 May 2017

Rev., 121, 764–787, doi:10.1175/1520-0493(1993)121<0764:PEOAUB>2.0.CO;2, 1993.

Han, J., and Pan, H. L.: Revision of convection and vertical diffusion schemes in the NCEP Global Forecast System, Wea. Forecasting, 26, 520–533, doi:10.1175/WAF-D-10-05038.1, 2011.

Han, J., Witek, M. L., Teixeira, J., Sun, R., Pan, H. L., Fletcher, J. K., and Bretherton, C. S.: Implementation in the NCEP GFS of a Hybrid Eddy-Diffusivity Mass-Flux (EDMF) boundary layer parameterization with dissipative heating and modified stable boundary layer mixing, Wea. Forecasting, 31(1), 341–352, doi:10.1175/WAF-D-15-0053.1, 2016.

Hong, S. Y., and Pan, H. L.: Nonlocal boundary layer vertical diffusion in a medium-range forecast model, Mon. Wea. Rev., 124, 2322–2339, doi:10.1175/1520-0493(1996)124<2322:NBLVDI>2.0.CO;2, 1996.

Intergovernmental Panel on Climate Change: Climate Change 2013: The Physical Science Basis, in Contribution of Working Group I to the Fifth Assessment Report of the Intergovernmental Panel on Climate Change, Cambridge Univ. Press, Cambridge, U. K., 2013.

Jiang, H., Xue, H., Teller, A., Feingold, G., and Levin, Z.: Aerosol effects on the lifetime of shallow cumulus, Geophys. Res. Lett., 33(14), doi:10.1029/2006gl026024, 2006.

Jiang, M., Li, Z., Wan, B., and Cribb, M.: Impact of aerosols on precipitation from deep convective clouds in eastern China, J. Geophys. Res. Atmos., 121(16), 9607–9620, doi:10.1002/2015JD024246, 2016.

Kanamitsu, M.: Description of the NMC Global Data Assimilation and Forecast System, Wea. Forecasting, 4(3), 335–342, doi:10.1175/1520-0434(1989)004<0335:DOTNGD>2.0.CO;2, 1989.

Khain, A, Benmoshe, N., and Pokrovsky, A.: Factors determining the impact of aerosols on surface precipitation from clouds: An attempt at classification, J. Atmos. Sci., 65(5), 1721–1748, doi:10.1175/2007JAS2515.1, 2008.

Koren, I., Kaufman, Y. J., Rosenfeld, D., Remer, L. A., and Rudich, Y.: Aerosol invigoration and restructuring of Atlantic convective clouds, Geophys. Res. Lett., 32(14), doi: 10.1029/2005gl023187, 2005.

Koren, I., Martins, J. V., Remer, L. A., and Afargan, H.: Smoke invigoration versus inhibition of clouds over the Amazon, Science, 321(5891), 946–949, doi:10.1126/science.1159185, 2008.

Li, Z., Niu, F., Fan, J., Liu, Y., Rosenfeld, D., and Ding, Y.: Long-term impacts of aerosols on the vertical development of clouds and precipitation, Nat. Geosci., 4(12), 888–894, doi:10.1038/ngeo1313, 2011.

Li, Z., Lau, W. K.-M., Ramanathan, V., Wu, G., Ding, Y., Manoj, M. G., Liu, J., Qian, Y., Li, J., Zhou, T., Fan, J., Rosenfeld, D., Ming, Y., Wang, Y., Huang, J., Wang, B., Xu, X., Lee, S.-S., Cribb, M., Zhang, F., Yang, X., Zhao, C., Takemura, T., Wang, K., Xia, X., Yin, Y., Zhang, H., Guo, J., Zhai, P. M., Sugimoto, N., Babu, S. S., and Brasseur, G. P.: Aerosol and monsoon climate interactions over Asia, Rev. Geophys., 54(4), 866–929, doi:10.1002/2015RG000500, 2016.

Lin, Y., and Zhao, C.: Trends of precipitation of different intensity in China, Acta Scientiarum Naturalium Universitatis Pekinensis, 45, 995–1002, 2009.

Lin, J. C., Matsui, T., Pielke, R. A., and Kummerow, C.: Effects of biomass-burning-derived aerosols on precipitation and clouds in the Amazon Basin: a satellite-based empirical study, J. Geophys. Res. Atmos., 111(D19), doi:10.1029/2005jd006884, 2006.

Molod, A., Takacs, L., Suarez, M., Bacmeister, J., Song, I. S., and Eichmann, A.: The GEOS-5 atmospheric general circulation model: mean climate and development from MERRA to Fortuna, NASA Tech. Rep. Series on Global Modeling and Data Assimilation, NASA TM—2012-104606, 28, 117 pp, 2012.

Molod, A., Takacs, L., Suarez, M., and Bacmeister, J.: Development of the GEOS-5 atmospheric general circulation model: evolution from MERRA to MERRA2, Geosci. Model Dev., 8, 1339–1356, doi:10.5194/gmd-8-1339-2015, 2015.

Moorthi, S., Pan, H. L., and Caplan, P.: Changes to the 2001 NCEP operational MRF/AVN global analysis/forecast system, NWS Technical Procedures Bulletin, 484, available online at www. nws.noaa.gov/om/tpb/484.htm, 2001.

Niu, F., and Li, Z.: Systematic variations of cloud top temperature and precipitation rate with aerosols over the global tropics, Atmos. Chem. Phys., 12(18), 8491–8498, doi:10.5194/acp-12-8491-2012, 2012.

Pan, H. L., and Wu, W. S.: Implementing a mass flux convective parameterization package for the NMC Medium-Range Forecast model, NMC Office Note 409, 40 pp, 1995.

Atmos. Chem. Phys. Discuss., doi:10.5194/acp-2017-256, 2017
Manuscript under review for journal Atmos. Chem. Phys.
Discussion started: 2 May 2017

Peng, J., Li, Z., Zhang, H., Liu, J., and Cribb, M. C.: Systematic changes in cloud radiative forcing with aerosol loading for deep clouds in the tropics, J. Atmos. Sci., 73, 231–249, doi:10.1175/JAS-D-15-0080.1, 2016.

Randles, C. A., da Silva, A. M., Buchard, V., Darmenoy, A., Colarco, P. R., Aquila, V., Bian, H., Nowottnick, E. P., Pan, X., Smirnov, A., Yu, H., and Govindaraju, R.: The MERRA-2 Aerosol Assimilation, NASA Tech. Rep. Series on Global Modeling and Data Assimilation, NASA TM—2016-104606, 45, 156 pp, 2016.

Rienecker, M. M., Suarez, M. J., Gelaro, R., Todling, R., Bacmeister, J., Liu, E., Bosilovich, M. G., Schubert, S. D., Takacs, L., Kim, G. K., Bloom, S., Chen, J., Collins, D., Conaty, A., da Silva, A., Gu, W., Joiner, J., Koster, R. D., Lucchesi, R., Molod, A., Owens, T., Pawson, S., Pegion, P., Redder, C. R., Reichle, R., Robertson, F. R., Ruddick, A. G., Sienkiewicz, M., and Woollen, J.: MERRA: NASA's Modern-Era Retrospective Analysis for Research and Applications, J. Climate, 24(14), 3624–3648, doi:10.1175/JCLI-D-11-00015.1, 2011.

Rosenfeld, D.: Suppression of rain and snow by urban and industrial air pollution, Science, 287(5459), 1793–1796, doi:10.1126/science.287.5459.1793, 2000.

Rosenfeld, D., Dai, J., Yu, X., Yao, Z., Xu, X., Yang, X., and Du, C.: Inverse relations between amounts of air pollution and orographic precipitation, Science, 315, 1396–1398, doi:10.1126/science.1137949, 2007.

Rosenfeld, D., Lohmann, U., Raga, G.B., Dowd, C. D. O., Kulmala, M., Fuzzi, S., Reissell, A., and Andreae, M. O.: Flood or drought: How do aerosols affect precipitation?, Science, 321(5894), 1309–1313, doi:10.1126/science.1160606, 2008.

Sela, J.: Implementation of the sigma pressure hybrid coordinate into GFS; NCEP Office, Note # 461, available at http://www.emc.ncep.noaa.gov/officenotes/FullTOC.html#2000, 2009.

Sundqvist, H., Berge, E., and Kristjansson, J. E.: Condensation and cloud parameterization studies with a mesoscale numerical weather prediction model, Mon. Wea. Rev., 117, 1641–1657, doi:10.1175/1520-0493(1989)117<1641:CACPSW>2.0.CO%3B2, 1989.

Tao, W. K., Chen, J. P., Li, Z., Wang, C., and Zhang, C.: Impact of aerosols on convective clouds and precipitation, Rev. Geophys., 50(2), doi:10.1029/2011rg000369, 2012.

Troen, I., and Mahrt, L.: A simple model of the atmospheric boundary layer: Sensitivity to surface

Atmos. Chem. Phys. Discuss., doi:10.5194/acp-2017-256, 2017
Manuscript under review for journal Atmos. Chem. Phys.
Discussion started: 2 May 2017

evaporation, Bound.-Layer Meteor., 37, 129–148, doi: 10.1007/BF00122760, 1986.

Twomey, S. A., Piepgrass, M., and Wolfe, T. L.: An assessment of the impact of pollution on global cloud albedo, Tellus B, 36(5), 356–366, doi:10.1111/j.1600-0889.1984.tb00254.x, 1984.

van den Heever, S. C., Stephens, G. L., and Wood, N. B.: Aerosol indirect effects on tropical convection characteristics under conditions of radiative–convective equilibrium, J. Atmos. Sci., 68(4), 699–718, doi: http://dx.doi.org/10.1175/2010JAS3603.1, 2011.

Wu, W. S., Purser, R. J., and Parrish, D. F.: Three-dimensional variational analysis with spatially inhomogeneous covariances, Mon. Wea. Rev., 130, 2905–2916, doi:10.1175/1520-0493(2002)130<2905:TDVAWS>2.0.CO;2, 2002.

Xie, P. P., Yatagai, A., Chen, M. Y., Hayasaka, T., Fukushima, Y., Liu, C. M., and Yang, S.: A gauge-based analysis of daily precipitation over East Asia, J. Hydrometeorol., 8(3), 607–626, doi:10.1175/Jhm583.1, 2007.

Xu, K. M., and Randall, D. A.: A semi-empirical cloudiness parameterization for use in climate models, J. Atmos. Sci., 53, 3084–3102, doi: 10.1175/1520-0469(1996)053<3084:ASCPFU>2.0.CO;2, 1996.

Xue, H., and Feingold, G.: Large-eddy simulations of trade wind cumuli: investigation of aerosol indirect effects, J. Atmos. Sci., 63(6), 1605–1622, doi:10.1175/JAS3706.1, 2006.

Yang, F. L., Pan., H. L., Krueger, S. K., Moorthi, S., and Lord, S. J.: Evaluation of the NCEP Global Forecast System at the ARM SGP site, Mon. Wea. Rev., 134(12), 3668–3690, doi:10.1175/MWR3264.1, 2006.

Yoo, H., and Li, Z.: Evaluation of cloud properties in the NOAA/NCEP global forecast system using multiple satellite products, Clim. Dyn., 39, 2769–2787, doi:10.1007/s00382-012-1430-0, 2012.

Yoo, H., Li, Z., Hou, Y.-T, Lord, S., Weng, F., and Barker, H. W.: Diagnosis and testing of low-level cloud parameterizations for the NCEP/GFS model satellite and ground-based measurements, Clim. Dyn., 41, 1595–1613, doi:10.1007/s00382-013-1884-8, 2013.

Zhao, Q. Y., and Carr, F. H.: A prognostic cloud scheme for operational NWP models, Mon. Wea. Rev., 125, 1931–1953, doi:10.1175/1520-0493(1997)125<1931:APCSFO>2.0.CO;2, 1997.

Figures and Tables

Table 1. Definitions of warm- and cold-base mixed-phase clouds and liquid clouds.

	Cloud-base temperature (ºC)	Cloud-top temperature (ºC)
Deep mixed-phase clouds with warm bases	> 15	< -4
Shallow mixed-phase clouds with cold bases	0–15	< -4
Liquid clouds	> 0	> 0

Table 2. Contingency table.

Observed / Forecast	Observed yes	Observed no
Forecast yes	Hits	False alarms
Forecast no	Misses	Correct negatives

Table 3. Correlation coefficients from linear regressions of visibility and different rain amount types for all seasons.

Rain rate / Season	Light rain	Moderate rain	Heavy rain	Very heavy rain	Rain amount
Spring	0.48*	0.51*	0.48*	0.17	0.40*
Summer	0.08	-0.16	-0.28	-0.41*	-0.38*
Autumn	0.31	0.18	0.26	-0.22	0.11
Winter	0.55*	0.26	0.26	0.27	0.29

* Values with an asterisk represent data at a confidence level greater than 95%.

Table 4. Correlation coefficients from linear regressions of visibility and different occurrence frequencies of rain amount type for all seasons.

Rain rate / Season	Light rain	Moderate rain	Heavy rain	Very heavy rain	Rain amount
Spring	0.61*	0.51*	0.38*	0.08	0.67*
Summer	0.23	-0.13	-0.26	-0.44*	-0.04
Autumn	0.52*	0.18	0.25	-0.10	0.45*
Winter	0.55*	0.22	0.20	-0.05	0.49*

* Values with an asterisk represent data at a confidence level greater than 95%.

Atmos. Chem. Phys. Discuss., doi:10.5194/acp-2017-256, 2017
Manuscript under review for journal Atmos. Chem. Phys.
Discussion started: 2 May 2017

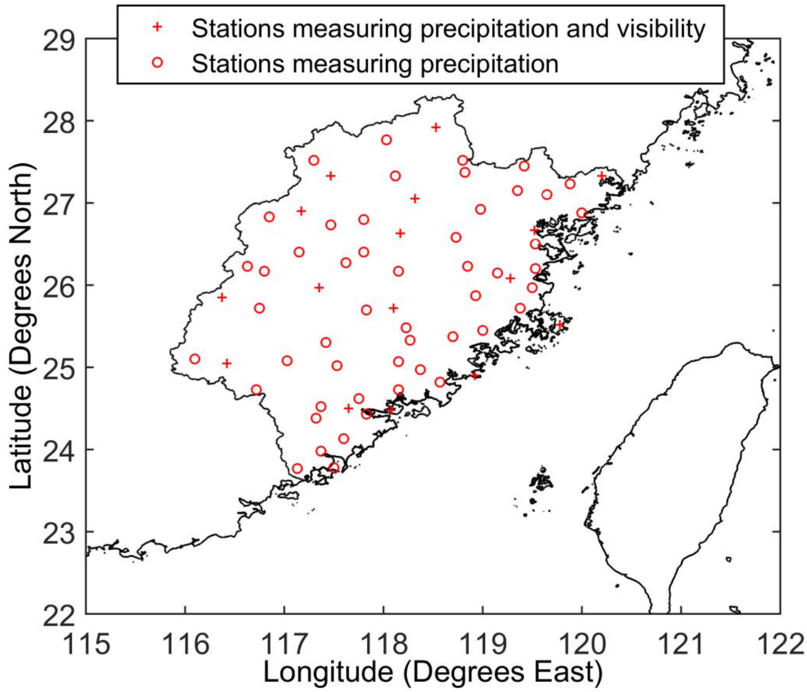

Fig. 1. Locations of 67 stations measuring precipitation in Fujian Province. Plus symbols show the locations of the 16 stations where visibility measurements are also made. This figure was plotted using the equidistant cylindrical projection.

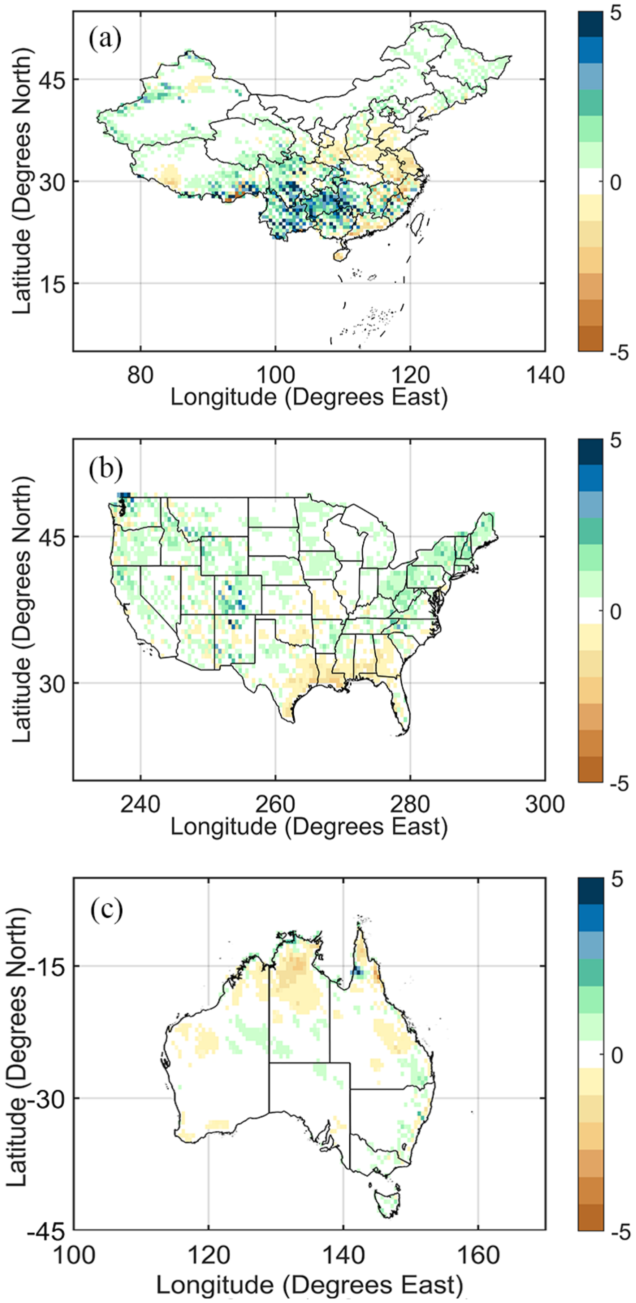

Fig. 2. Annual mean precipitation differences (in mm d^{-1}) between the GFS model forecast and the CPC analysis in three countries: (a) China, (b) the contiguous U.S., and (c) Australia. Data are from the year 2015. This figure was plotted using the equidistant cylindrical projection.

Atmos. Chem. Phys. Discuss., doi:10.5194/acp-2017-256, 2017
Manuscript under review for journal Atmos. Chem. Phys.
Discussion started: 2 May 2017

Atmospheric Chemistry and Physics
Open Access
Discussions

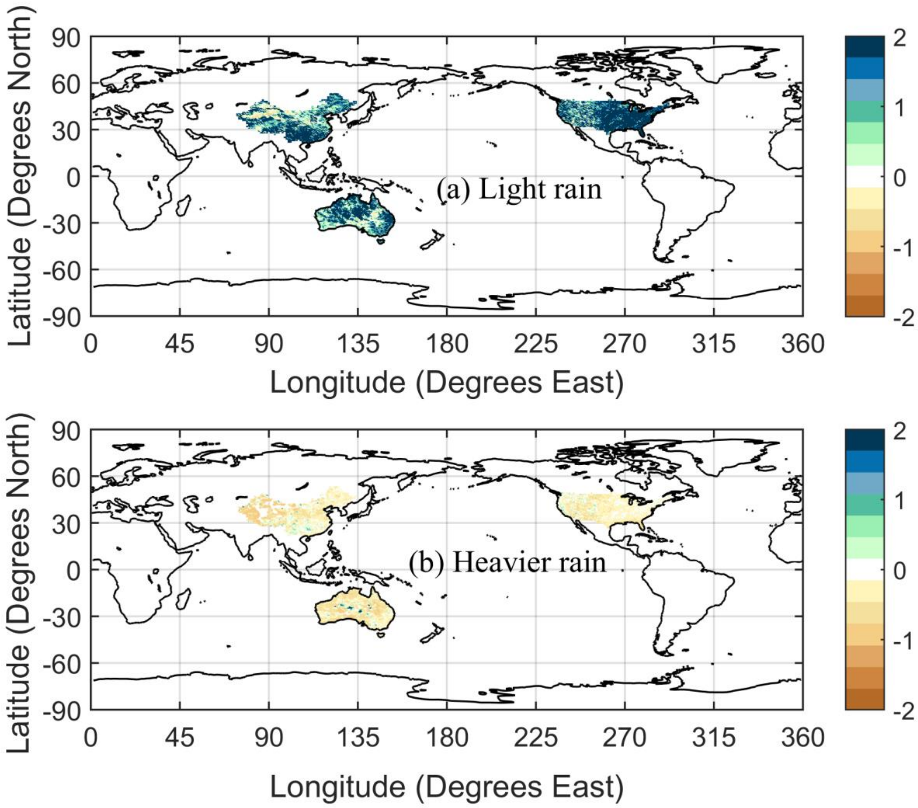

786

787 **Fig. 3.** Annual mean relative difference (in mm d^{-1}) between forecast and observed
788 precipitation for (a) light rain (< 10 mm d^{-1}) and (b) heavier rain (> 10 mm d^{-1}). Data
789 are from the year 2015. This figure was plotted using the equidistant cylindrical
790 projection.

791

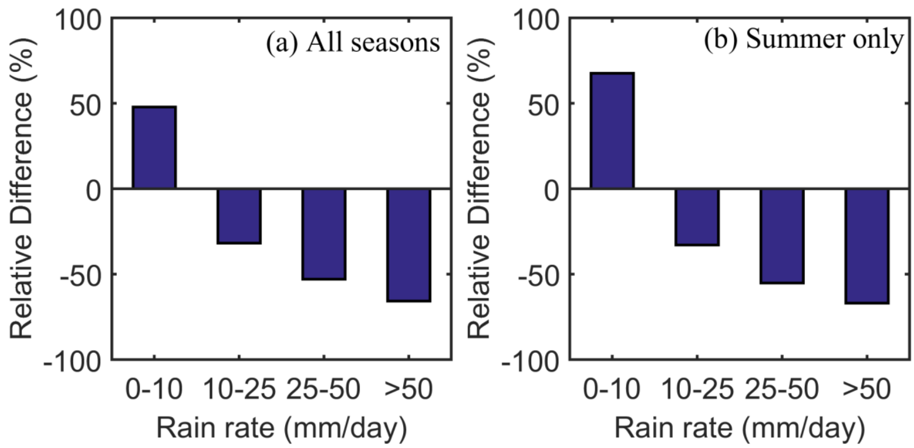

Fig. 4. Mean relative difference in precipitation between forecast and observed daily light (< 10 mm d^{-1}), moderate (10–25 mm d^{-1}), heavy (25–50 mm d^{-1}), and very heavy (> 50 mm d^{-1}) rain amounts for (a) all seasons and (b) summer only. Data are from the year 2015 and from the three countries considered in the study.

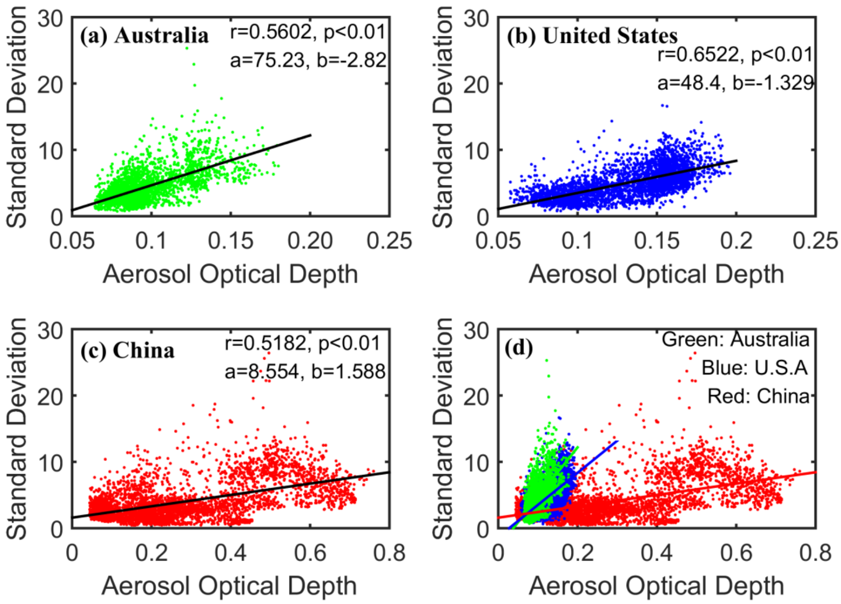

798

799 **Fig. 5.** Standard deviations of the daily precipitation difference as a function of
800 aerosol optical depth for (a) Australia (green points), (b) the United States (blue
801 points), (c) China (red points), and (d) all three countries. Data are from the year
802 2015.

803

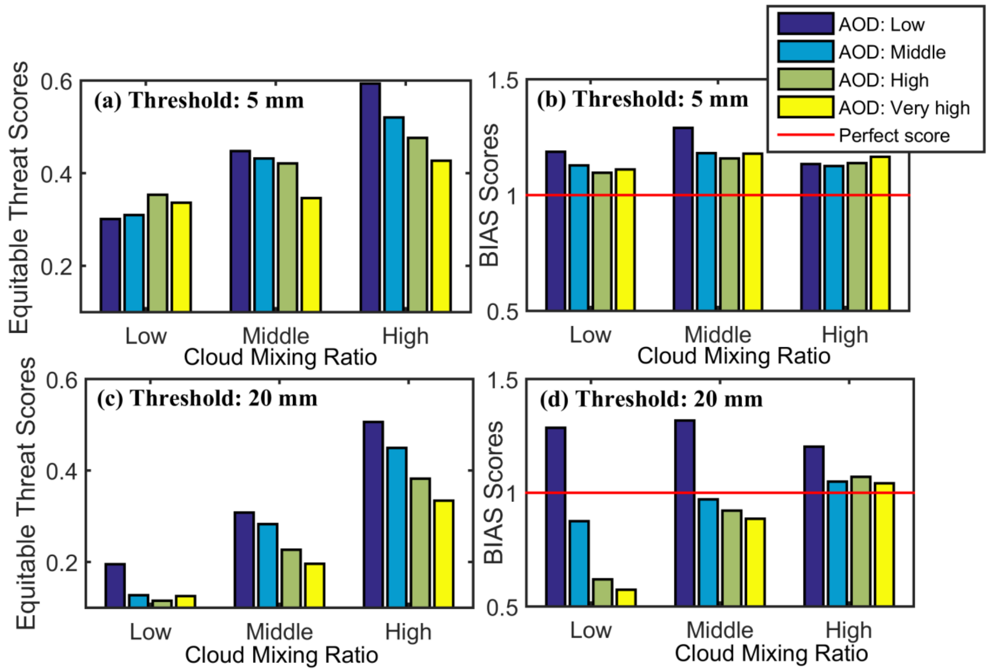

Fig. 6. ETS scores (a, c) and BIAS scores (c, d) in different AOD bins for certain cloud mixing ratio conditions. AOD is equally divided into four bins (low: dark blue bars; middle: blue bars; high: green bars; and very high: yellow bars). Cloud mixing ratios are equally divided into three categories (low, middle, and high). Data are from the year 2015 in the U.S. The horizontal red lines in (b) and (d) represent perfect scores.

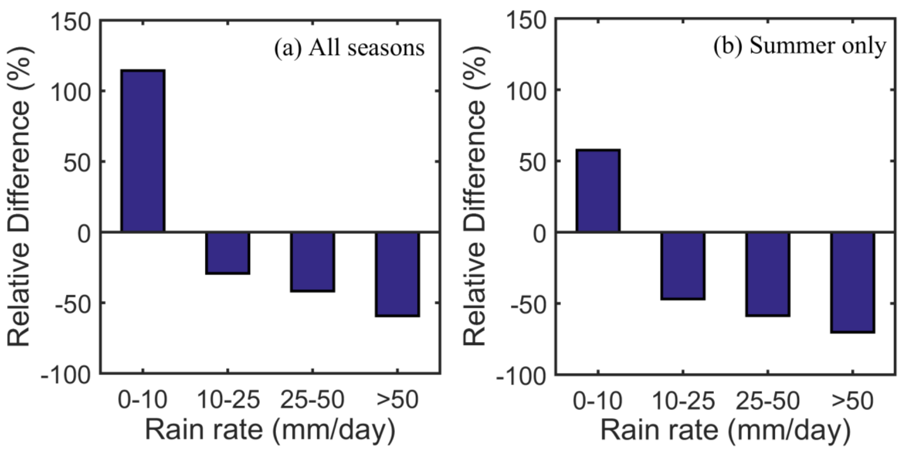

Fig. 7. Mean relative precipitation differences between forecast and observed daily light (< 10 mm d^{-1}), moderate (10–25 mm d^{-1}), heavy (25–50 mm d^{-1}), and very heavy (> 50 mm d^{-1}) rain amounts for (a) all seasons and (b) summer only in Fujian Province, China. Data are from 1985–2010.

Atmos. Chem. Phys. Discuss., doi:10.5194/acp-2017-256, 2017
Manuscript under review for journal Atmos. Chem. Phys.
Discussion started: 2 May 2017

Atmospheric Chemistry and Physics
Open Access
Discussions

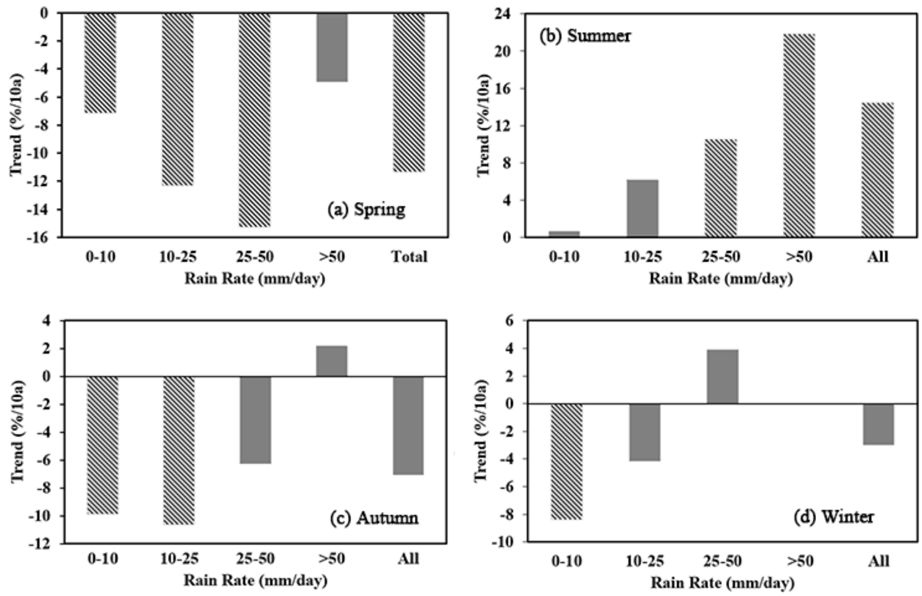

Fig. 8. Trends (percent change per decade) in mean daily light rain (< 10 mm d^{-1}), moderate rain (10–25 mm d^{-1}), heavy rain (25–50 mm d^{-1}), very heavy rain (> 50 mm d^{-1}), and total rain amounts for (a) spring, (b) summer, (c) autumn, and (d) winter in Fujian Province, China. Data are from 1980–2009. Cross-hatched bars represent data at a confidence level greater than 95%.

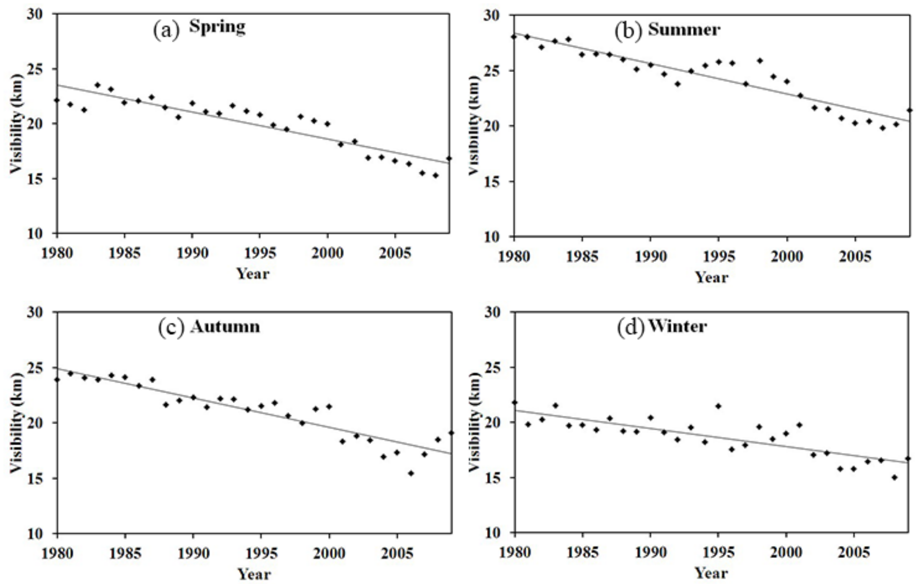

Fig. 9. Annual mean visibilities in (a) spring, (b) summer, (c) autumn, and (d) winter in Fujian Province, China. Data are from 1980–2009. Least squares regression lines at the 95% confidence level are shown.

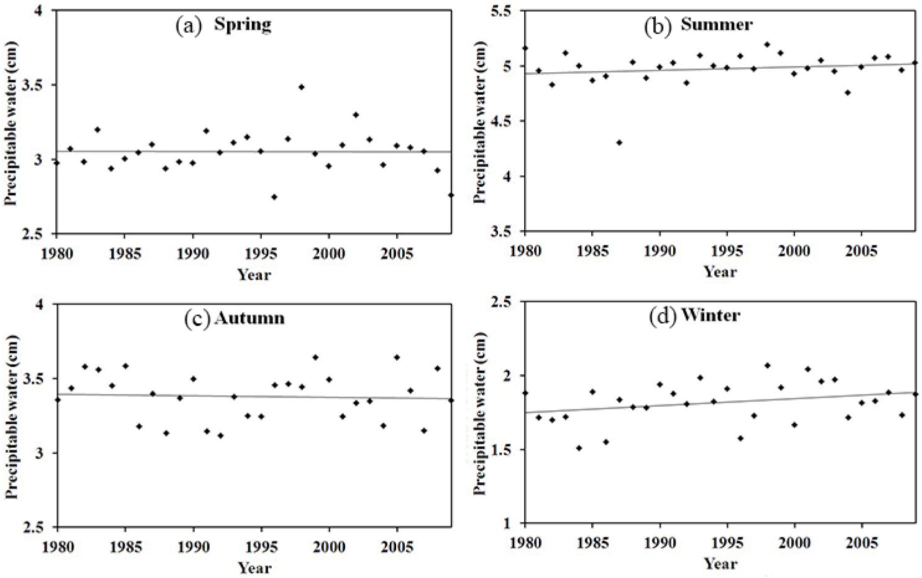

832

833 **Fig. 10.** Same as Fig. 9, except for precipitable water vapor.

834

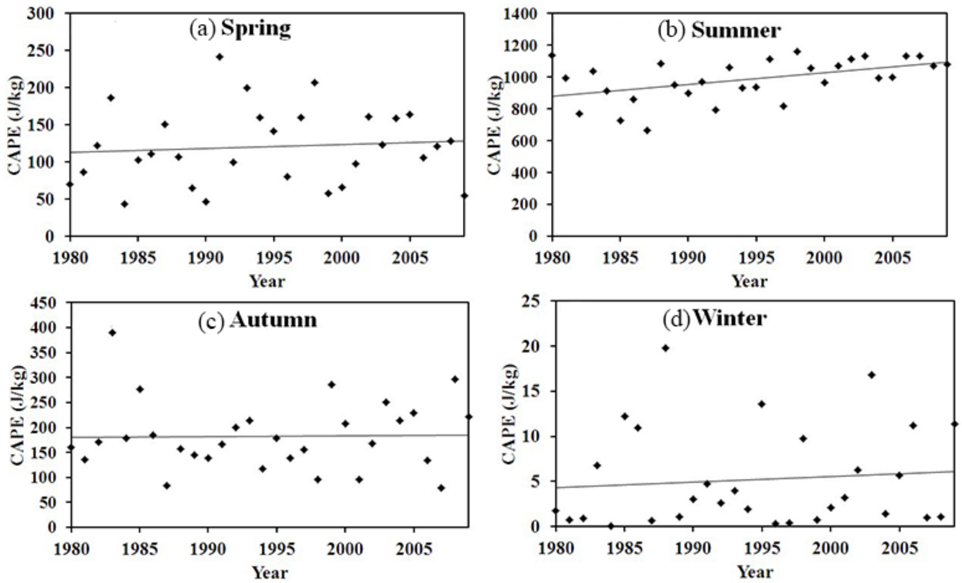

Fig. 11. Same as Fig. 9, except for CAPE.

Atmos. Chem. Phys. Discuss., doi:10.5194/acp-2017-256, 2017
Manuscript under review for journal Atmos. Chem. Phys.
Discussion started: 2 May 2017

Atmospheric Chemistry and Physics
Open Access
Discussions

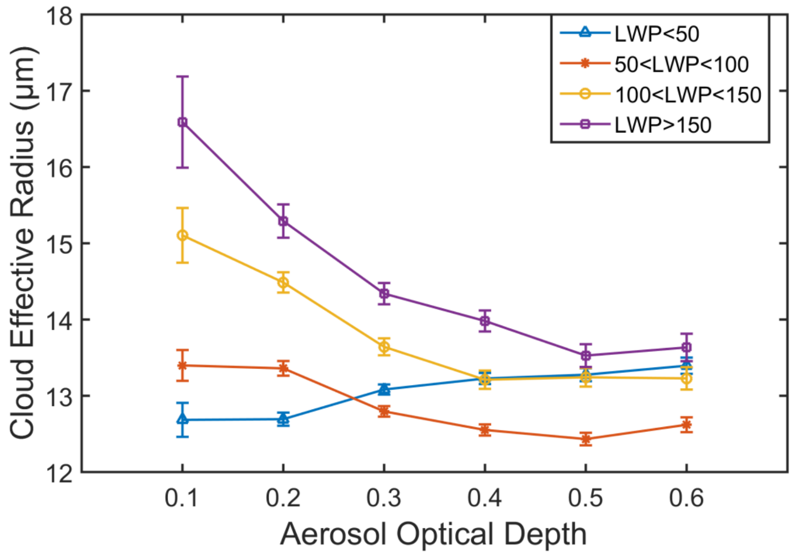

Fig. 12. Cloud effective radius as a function of AOD for liquid clouds (clouds with top temperatures greater than 273 K) in Fujian Province, China. Blue triangles represent cases where the LWP is less than 50 g m^{-2}, orange stars represent LWPs between 50 g m^{-2} and 100 g m^{-2}, yellow circles represent LWPs between 100 g m^{-2} and 150 g m^{-2}, and purple squares represent LWPs greater than 150 g m^{-2}. Error bars represent one standard error. Data are from 2003–2012.

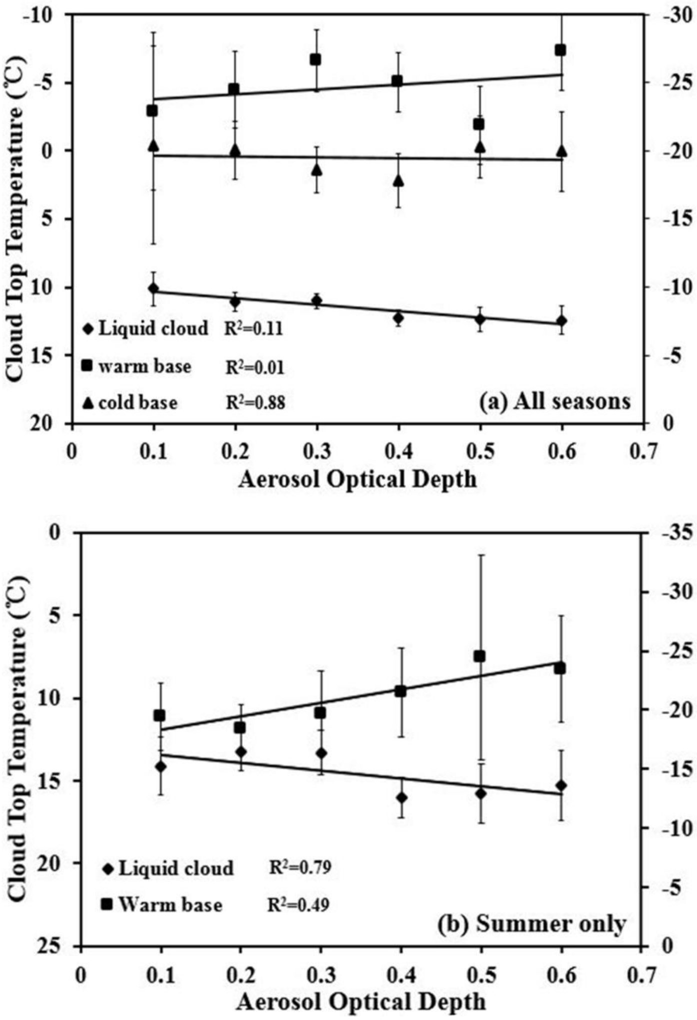

Fig. 13. Cloud-top temperature as a function of AOD for (a) liquid, warm-base mixed-phase, and cold-base mixed-phase clouds in all seasons, and (b) liquid and warm-base mixed-phase clouds in summer in Fujian Province, China. Diamonds represent liquid clouds, squares represent warm-base mixed-phase clouds, and triangles represent cold-base mixed-phase clouds. Right-hand ordinates are for warm-base and cold-base mixed-phase clouds. Data are from 2006–2010.

Atmos. Chem. Phys. Discuss., doi:10.5194/acp-2017-256, 2017
Manuscript under review for journal Atmos. Chem. Phys.
Discussion started: 2 May 2017

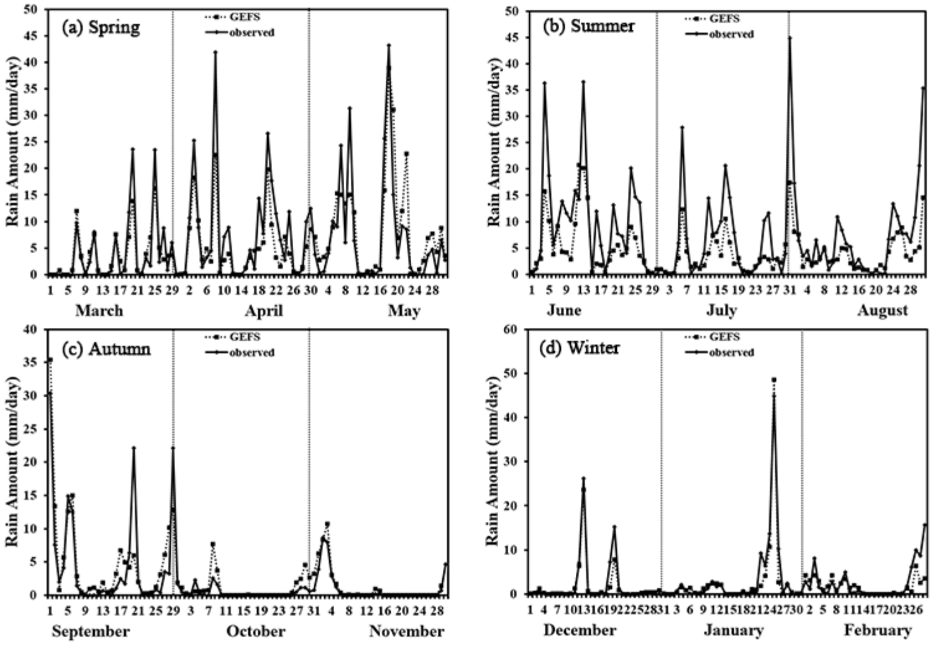

Fig. 14. Time series of regionally-averaged daily rainfall amount in Fujian Province, China in (a) spring, (b) summer, (c) autumn, and (d) winter. Dotted lines represent rainfall forecasts from the GEFS and solid lines represent rainfall measurements from gauge-based observations. Data are from 2001.